Title

Optical injection locking of a THz quantum-cascade VECSEL with an electronic source.

Journal

Optics Letters, 48(14)

ISSN

0146-9592

Authors

Curwen, Christopher A
Kim, Anthony D
Karasik, Boris S
et al.

Publication Date

2023-07-15

DOI

10.1364/ol.492182

Optical injection locking of a THz quantum-cascade VECSEL with an electronic source

CHRISTOPHER A. CURWEN,[1,*] ANTHONY D. KIM,[2] BORIS S. KARASIK,[1] JONATHAN H. KAWAMURA,[1] AND BENJAMIN S. WILLIAMS[2]

[1]*Jet Propulsion Laboratory, California Institute of Technology, Pasadena, CA 91109, USA*
[2]*Department of Electrical and Computer Engineering, University of California, Los Angeles, CA 90095 USA*
**Corresponding author: chris.a.curwen@jpl.nasa.gov*

Received XX Month XXXX; revised XX Month, XXXX; accepted XX Month XXXX; posted XX Month XXXX (Doc. ID XXXXX); published XX Month XXXX

Optical injection locking of a metasurface quantum-cascade (QC) vertical-external-cavity surface-emitting-laser (VECSEL) is demonstrated at 2.5 THz using a Schottky diode frequency multiplier chain as the injection source. The spectral properties of the source are transferred to the laser output with a locked linewidth of ~1 Hz, as measured by a separate subharmonic diode mixer, and a locking bandwidth of ~300 MHz is achieved. The large locking range is enabled by the microwatt power levels available from modern diode multipliers. The interplay between the injected signal and feedback from external reflections is studied and demonstrated to increase or decrease locking bandwidth relative to the classic locking range depending on the phase of the feedback.

Tunable, single-mode terahertz (THz) quantum-cascade lasers (QCLs) have many potential spectroscopic applications thanks to the abundance of strong molecular and atomic transitions in the THz frequency range [1, 2]. Their milliwatt-level output power makes them attractive candidates for local oscillators to pump mixer arrays in heterodyne instruments in the 2-6 THz range for astrophysical and space science [3, 4]. However, the free-running frequency of THz QCLs (and most semiconductor lasers) is often too unstable to achieve the spectral resolution necessary for applications of interest. This requires the QCL to be locked to a more stable reference. For THz QCLs, this has typically been performed by down-converting the THz laser signal to generate an RF intermediate frequency (IF) that can be locked to a reference using a phase-locked loop. For example, this was achieved by mixing the QCL signal with a tone of a subharmonic Schottky diode mixer [5-7] or superlattice mixer [8]. Locking to the output of a 1.5 THz and 2.7 THz Schottky diode frequency multiplier chain (FMC) has also been demonstrated utilizing cryogenic superconducting mixers [9, 10]. Optical frequency combs have also been used to lock THz QCLs via generation of an RF beat note in a photoconductive mixer [11], electrooptic sampling in a ZeTe crystal [12], or a superconducting mixer [13].

A different approach for stabilization is to directly injection lock a THz QCL with a more stable THz source. This approach is usually challenging because of the lack of sufficiently powerful THz sources. The only previous demonstration was a photonic approach in which the THz injection signal was generated by a photoconductive antenna driven by the beat note of two infrared diode lasers locked to the teeth of an optical frequency comb [14, 15]. However, electronic sources – such as Schottky diode frequency multiplier chains (FMCs) – have reached a level of maturity that tens of microwatts of THz power can be generated at frequencies above 2 THz [16], where THz QCLs operate. In this Letter, we report direct injection locking of a THz QC vertical-external-cavity surface-emitting laser (VECSEL) to the output of a frequency-agile diode FMC source at 2.5 THz. The high power from the FMC source allows for large locking bandwidths compared to the free-running linewidth of the laser.

The experimental setup is illustrated in Fig. 1(a), and a simplified schematic is shown in Fig. 1(b). The FMC source is similar (but not identical) to that in [17] and consists of a 15.43 GHz synthesized signal, followed by a ×6 multiplying amplifier (Millitech AMC-1C-RFH00), a 100 GHz power amplifier [18], and three more frequency triplers [17-19] for a total multiplication factor of ×162. The source output ~7 μW at 2.5 THz and is coupled to the QC-VECSEL via off-axis parabolic (OAP) mirrors. The output of the QC-VECSEL is monitored with high-spectral resolution via a 3 μm thick Mylar beam splitter that diverts a small portion of the QC-VECSEL output to a subharmonic diode mixer. The mixer (based on design in [7]) is pumped by a 100 GHz LO chain and the QC-VECSEL signal mixes with the 25th harmonic. The IF from the mixer is amplified by 60 dB and sent to a Keysight PXA signal analyzer. The two synthesizers for the FMC and mixer were locked to a common 10 MHz quartz reference oscillator. No optical isolators are available for this frequency range, however, since the FMC is not a fundamental oscillator, mutual injection-locking is not an issue.

As well as the use of an all-electronic THz source, the use of the

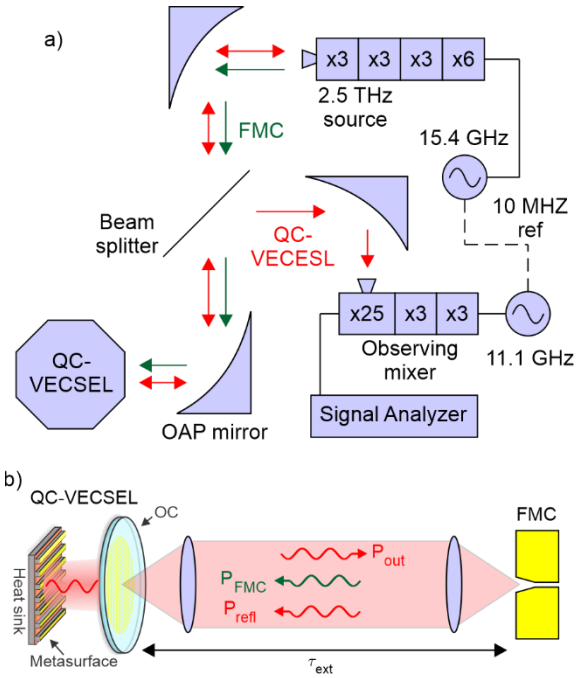

Fig. 1. (a) Block diagram of injection locking experimental setup. Beam paths for the QC-VECSEL and FMC are indicated with red and green arrows, respectively. (b) Simplified illustration emphasizing relevant coupled fields.

external-cavity QC-VECSEL [20] rather than a ridge waveguide adds a novel component to this study. The QC-VECSEL is based on a metasurface reflectarray of metal-metal waveguide patch antennas loaded with QC gain material that amplifies and reflects normally incident THz radiation. A laser is formed by incorporating the metasurface amplifier into an external cavity that provides sufficient feedback to enable oscillation. A key advantage of the QC-VECSEL approach is that the large radiating area of the metasurface supports a high-quality, near-Gaussian beam in the external cavity, overcoming an issue that has plagued ridge-waveguide devices with subwavelength facet emitters [21]. This point is also interesting for the prospects of injection locking as it is potentially easier to couple the injected signal power to the large surface-radiating area of the VECSEL compared to the facet of a ridge waveguide. In [14], <10% of the injected THz power was assumed to be coupled to the QCL due to mode mismatch between the free-space beam and the surface-plasmon ridge waveguide mode, and the situation would be worse for a metal-metal waveguide, which is the preferred technology for high-temperature operation [22]. Additionally, both QC-VECSEL and FMC sources have shown broadband frequency tunability (>10%) [17, 23], potentially enabling a broadband locked setup.

The metasurface and VECSEL cavity used in this study are the same as in [5]. The metasurface consists of an array of narrow metal-metal ridge waveguides spaced with a subwavelength periodicity (85 μm), and loaded with THz QC gain material. The active region is based on that in [24] and is grown 5 μm thick for improved continuous-wave operation (the layer sequence is given in [25]). The ridge antennas are coupled to surface radiation where the resonant frequency of 2.5 THz is determined by the width of the ridges (17.4 μm). The metasurface has a total area of 2×2 mm^2, but only a circular area 0.8 mm in diameter is biased. Additionally, the widths of the ridges are spatially varying to create a focusing phase profile with a focal length of 7 mm [21]. The metasurface is mounted

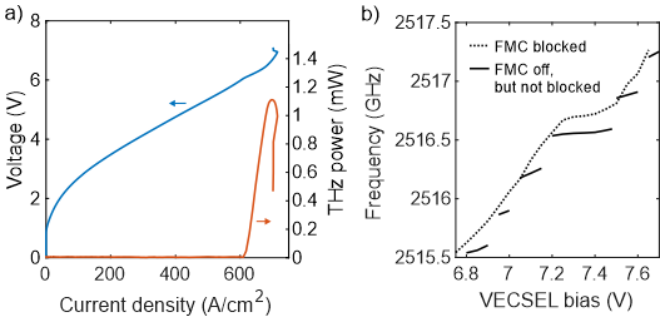

Fig. 2. (a) QC-VECSEL voltage and output power versus current density. (b) Lasing frequency as a function of bias on the QC-VECSEL with and without feedback from reflections at the FMC waveguide block. Note: gaps in the data with the FMC not blocked are a result of recording the data at a set of discrete points, not due to a lack of lasing

in an external cavity that has a fixed cavity length and uses a set of three screws and springs to attach and align the output coupler (feedback mirror) in a kinematic manner. The output coupler is made in-house and consists of a mesh of 3 μm wide metal lines deposited at a 15 μm pitch on a 200 μm thick z-cut crystal quartz substrate and has a transmission of ~12% at 2.5 THz. The QC-VECSEL cavity was ~450 μm long and lasing occurred at 2.51 THz. The current, voltage, and output power data for the QC-VECSEL are plotted in Fig. 2(a). The device emits ~1.2 mW of continuous wave THz power at 77 K.

In Fig. 2(b), the free-running QC-VECSEL frequency as a function of bias is plotted with and without the FMC aligned, but with the FMC output off in both cases. Without the FMC aligned, the frequency tuning is continuous, but with the FMC aligned, the frequency tuning becomes largely discrete with small amounts of continuous tuning around steps spaced by ~330 MHz. This is the standard behavior for a laser locked to time-delayed feedback associated with reflections of the QC-VECSEL signal at the FMC block, as described in [26, 27]. This feedback is illustrated in Figs. 1(a) and (b). The discrete frequencies correspond to frequencies where the round-trip phase accumulation between the QC-VECSEL and the FMC (τ_{ext}) is a multiple of 2π; the spacing between these frequencies is given by $\Delta f_{refl} = 1/\tau_{ext}$. The discrete hopping observed indicates that $\kappa\tau_{ext}\sqrt{P_{refl}/P_{out}} > 1$, which is the point when multiple solutions occur for a single free-running frequency. P_{refl} is the power of the reflected signal fed back into the QC-VECSEL, P_{out} is the output power of the QC-VECSEL, and $\kappa = \omega_{lase}/2Q$ is the coupling efficiency between the fed-back signal and the VECSEL, where ω_{lase} is the lasing frequency, and Q is the quality factor of the VECSEL cavity. In our setup, $Q \approx 200, \tau_{ext} =$ 3 ns, and $P_{out} = 1$ mW at 2.5 THz, so the feedback power should at least be 70 nW.

In Fig. 3(a), the output of the FMC is turned on, and average IF spectra from the diode mixer are recorded as the FMC output frequency is swept across the QC-VECSEL lasing frequency. The averaged free-running VECSEL signal is observed as a broad feature in the center of the figures (3 dB linewidth on the order of 10 MHz, but occasional excursions over 100 MHz). The sharp diagonal feature sweeping across the figures is the injected tone. When the injected frequency is close enough to the free-running frequency of the QC-VECSEL, the frequency of the laser is pulled, and becomes locked to the FMC and takes on the FMC's narrow-band spectral properties, as shown in Fig. 3(c). The locked linewidth is ~1 Hz with ~40 dB SNR. Sidebands around 20-30 dB below the main tone are

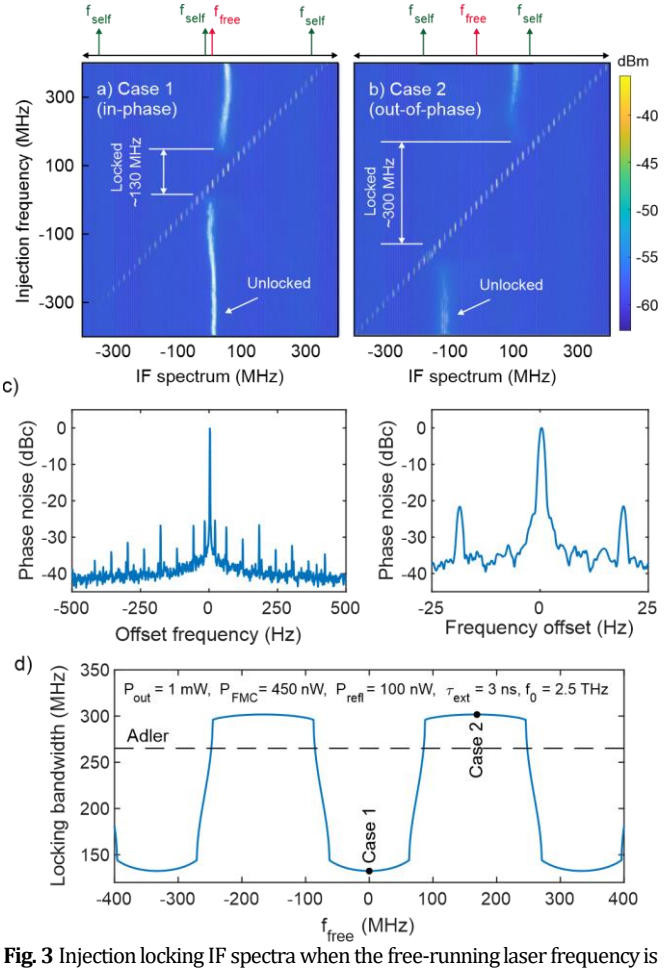

Fig. 3 Injection locking IF spectra when the free-running laser frequency is aligned with (a) in-phase feedback and (b) out-of-phase feedback. Axes represent relative frequency, not absolute. (c) High spectral resolution measurements of locked QC-VECSEL linewidth (signal analyzer resolution bandwidth set to 1 Hz). (d) Simulated locking bandwidth as a function of free-running laser frequency. The classic Adler locking range is indicated with a dashed line for reference.

observed at harmonics and subharmonics of 60 Hz, which likely originate from the FMC experiencing power line pick up from the reference source, as observed in [17]. The SNR is limited by the FMC, which is degraded by a factor of $20\times\log_{10}(162) = 44$ dB compared to the starting RF synthesizer SNR. It is noted that the FMC signal is still visible, even when detuned from the QC-VECSEL frequency, this is presumably because the VECSEL amplifies the off-resonant FMC signal, not because any portion of the laser power is locked to the FMC.

Traditionally, the locking bandwidth as a result of an injected signal is given by the Adler expression, which is proportional to the square root of the ratio of the injected power to the output power of the laser, $\Delta\omega_{Adler} = 2\kappa\sqrt{P_{inj}/P_{out}}$ [28]. However, in our setup, we observe that the locking bandwidth changes depending on the distance from the QC-VECSEL to the FMC, despite a constant κ, P_{inj}, and P_{out}. This is because the locking bandwidth depends on the the phase of the feedback from reflections at the FMC block. Consider the two measured cases in Fig. 3(a) and (b). Between the two sweeps, the biases on the QC-VECSEL and FMC are fixed (power levels are fixed), but the distance between the QC-VECSEL and FMC is tuned by a quarter wavelength (~30 μm) using a micrometer. This changes the alignment of the free-running QC-VECSEL frequency relative to the frequencies for in-phase feedback from reflections at the FMC block ($f_{refl} = m/\tau_{ext}$, where m is an integer). In Fig. 3(a), the free-running frequency is aligned with in-phase feedback, and in Fig. 3(b), the free-running frequency is aligned with out-of-phase feedback (round trip phase accumulation is an odd multiple of π). The locking range is larger when the free-running frequency is aligned with out-of-phase feedback. Qualitatively, this can be explained by the fact that locking is a result of reducing threshold gain for the laser at the injected signal. When the feedback is out-of-phase, this increases the threshold gain of the QC-VECSEL relative to the free-running case, making the laser more amenable to locking to gain reductions associated with the FMC injected signal. When the feedback is in-phase, this reduces the threshold gain relative to the free-running case, creating stronger competition with locking to the FMC injected signal.

Numerically, the problem can be modeled using the standard rate equation for the phase difference between the laser and the injected signal [29]:

$$\frac{d\phi(t)}{dt} = \frac{\alpha}{2}\{g[N(t) - N_{th}]\} - \kappa\sqrt{\frac{P_{inj}}{P_{out}(t)}}\sin\phi(t) - \Delta\omega \qquad (1)$$

where $\Delta\omega$ is the difference between the free-running and injection frequencies, $N(t)$ and N_{th} are the real-time and threshold number of carriers, g is the gain coefficient, and α is the linewidth enhancement factor, which we assume to be 0 for quantum-cascade lasers [30]. In the case of feedback from reflections at the mixer, the phase is fixed as $\phi_{refl} = \omega_{lock}\tau_{ext}$, and one can solve for $\Delta\omega$. In the case of external injection, we can select $\Delta\omega$ and solve for the necessary injection phase for locking, giving the standard Adler expression given above. To understand the locking conditions in the combined case, we can solve (1) with $\sqrt{P_{inj}}\sin\phi = \sqrt{P_{FMC}}\sin\phi_{FMC} + \sqrt{P_{refl}}\sin(\omega_{FMC}\tau_{ext})$, where P_{FMC}, ω_{FMC}, and ϕ_{FMC} are the power, frequency, and relative phase of the FMC signal. We find the phase condition:

$$\phi_{FMC} = \sin^{-1}\left\{-\frac{\Delta\omega}{\kappa}\sqrt{\frac{P_{out}}{P_{FMC}}} - \sqrt{\frac{P_{refl}}{P_{FMC}}}\sin(\omega_{FMC}\tau_{ext})\right\},$$

which gives the following limitation on the range of solutions for the lower ($\omega_{inj} < \omega_{free}$) and upper ($\omega_{inj} > \omega_{free}$) bands by setting the argument equal to plus and minus one, respectively:

$$\Delta\omega = \pm\kappa\sqrt{\frac{P_{FMC}}{P_{out}}}\left[1 \mp \sqrt{\frac{P_{refl}}{P_{FMC}}}\sin(\omega_{FMC}\tau_{ext})\right].$$

These are the same solutions as the typical injection locking bandwidth expression, but scaled by the terms in brackets, which oscillate sinusoidally around one as the free-running frequency scans relative to τ_{ext}. While the solution range for either sideband can be larger than that for typical injection locking by a factor of $1 + \sqrt{P_{refl}/P_{FMC}}$ when $\sin(\omega_{FMC}\tau_{ext}) = \pm 1$, the value of ω_{free} that satisfies this condition is different for the two sidebands, so the maximum solution range for a given ω_{free} is not simply $2 \times \left(1 + \sqrt{P_{refl}/P_{FMC}}\right)$. To determine the locking range, we must solve for the gain reduction at each frequency ($\Delta g_{th} \propto \sqrt{P_{inj}/P_{out}}\cos\phi$) with and without the FMC output on (feedback present in both cases) and compare.

In Fig. 3(d), the predicted locking range as a function of the free-running QC-VECSEL frequency is plotted assuming an FMC power of 450 nW, and a reflected power of 100 nW. This give a good agreement between the maximum and minimum locking ranges we observed experimentally and is also in agreement with the apparent strength of

the feedback based on the data in Fig. 2(b). This implies -13 dB coupling of the FMC to the QC-VECSEL. This low coupling efficiency suggests that the FMC and QC-VECSEL beams are not matched very well. The Adler locking range that would be expected without any feedback is indicated with a dashed line and is quite similar to $1/\tau_{ext}$. In this case, the injection locking range is largely unperturbed for most free-running frequencies, but it is reduced sharply when aligned well with in-phase feedback. If τ_{ext} were reduced and P_{refl} increased, the locking range could increase substantially for the given injection power (see Supplement). Or similarly, the existing setup would give a much larger boost in locking range (relative to the Adler expression) if P_{FMC} was smaller.

In conclusion, we have demonstrated direct injection locking of a THz QC-VECSEL using the output of a THz Schottky diode frequency multiplier chain. A locking range of >300 MHz is demonstrated thanks to the high injection power from the FMC. Locked linewidths are on the order of ~1 Hz, reflecting the spectral characteristics of the FMC. This large locking range is particularly useful when considering that, in practice, the laser should be locked with a small amount of the FMC power coupled in via a beam splitter, leaving most of the laser power available to the heterodyne instrument. Direct injection locking presents advantages over active stabilization schemes that use the bias on the laser to correct for error, such as reduced amplitude noise and broader locking bandwidth. Future work may explore the injection locking of broadly tunable VECSELs. With the ever-improving power, bandwidth, frequency coverage, and commercial availability of THz FMCs, we envision the possibility of hybrid electronic-photonic systems for coverage of frequencies from 2-6 THz for high precision spectroscopy applications.

Acknowledgments. This research was carried out, in part, at the Jet Propulsion Laboratory, California Institute of Technology, under a contract with the National Aeronautics and Space Administration. The quantum-cascade wafer material was grown by IQE PLC.

Disclosures. The authors declare no conflicts of interest.

Data availability. Data underlying the results presented in this paper are not publicly available at the this time but may be obtained from the authors upon reasonable request.

Supplemental document. See Supplement 1 for supporting content.

References

1. I. R. Medvedev, C. F. Neese, G. M. Plummer, and F. C. De Lucia, Opt. Lett. **35**, 1533-1535 (2010).
2. M. Naftaly, N. Vieweg, and A. Deninger, Sensors-Basel **19** (2019).
3. A. Khalatpour, A. K. Paulsen, S. J. Addamane, C. Deimert, J. L. Reno, Z. R. Wasilewski, and Q. Hu, IEEE Trans. Terahertz Sci. Technol. **12**, 144-150 (2022).
4. H. Richter, M. Wienold, L. Schrottke, K. Biermann, H. T. Grahn, and H. W. Hubers, IEEE Trans. Terahertz Sci. Technol. **5**, 539-545 (2015).
5. C. A. Curwen, J. H. Kawamura, D. J. Hayton, S. J. Addamane, J. L. Reno, B. S. Williams, and B. S. Karasik, TechRxiv. Preprint. (2023).
6. A. Danylov, N. Erickson, A. Light, and J. Waldman, Opt. Lett. **40**, 5090-5092 (2015).
7. A. A. Danylov, A. R. Light, J. Waldman, N. R. Erickson, X. F. Qian, and W. D. Goodhue, Opt. Express **20**, 27908-27914 (2012).
8. D. J. Hayton, A. Khudchencko, D. G. Pavelyev, J. N. Hovenier, A. Baryshev, J. R. Gao, T. Y. Kao, Q. Hu, J. L. Reno, and V. Vaks, Appl. Phys. Lett. **103** (2013).
9. P. Khosropanah, A. Baryshev, W. Zhang, W. Jellema, J. N. Hovenier, J. R. Gao, T. M. Klapwijk, D. G. Paveliev, B. S. Williams, S. Kumar, *et al.*, Opt. Lett. **34**, 2958-2960 (2009).
10. D. Rabanus, U. U. Graf, M. Philipp, O. Ricken, J. Stutzki, B. Vowinkel, M. C. Wiedner, C. Walther, M. Fischer, and J. Faist, Opt. Express **17**, 1159-1168 (2009).
11. M. Ravaro, C. Manquest, C. Sirtori, S. Barbieri, G. Santarelli, K. Blary, J. F. Lampin, S. P. Khanna, and E. H. Linfield, Opt. Lett. **36**, 3969-3971 (2011).
12. S. Barbieri, P. Gellie, G. Santarelli, L. Ding, W. Maineult, C. Sirtori, R. Colombelli, H. Beere, and D. Ritchie, Nat. Photon. **4**, 636-640 (2010).
13. S. Bartalini, L. Consolino, P. Cancio, P. De Natale, P. Bartolini, A. Taschin, M. De Pas, H. Beere, D. Ritchie, M. S. Vitiello*, et al.*, Phys. Rev. X **4** (2014).
14. J. R. Freeman, L. Ponnampalam, H. Shams, R. A. Mohandas, C. C. Renaud, P. Dean, L. H. Li, A. G. Davies, A. J. Seeds, and E. H. Linfield, Optica **4**, 1059-1064 (2017).
15. R. A. Mohandas, L. Ponnampalam, L. H. Li, P. Dean, A. J. Seeds, E. H. Linfield, A. G. Davies, and J. R. Freeman, Optica **7**, 1143-1149 (2020).
16. J. V. Siles, K. B. Cooper, C. Lee, R. H. Lin, G. Chattopadhyay, and I. Mehdi, IEEE Trans. Terahertz Sci. Technol. **8**, 596-604 (2018).
17. A. Maestrini, I. Mehdi, J. V. Siles, J. S. Ward, R. Lin, B. Thomas, C. Lee, J. Gill, G. Chattopadhyay, E. Schlecht*, et al.*, IEEE Trans. Terahertz Sci. Technol. **2**, 177-185 (2012).
18. A. Maestrini, J. S. Ward, C. Tripon-Canseliet, J. J. Gill, C. Lee, H. Javadi, G. C. Attopadhyay, and I. Mehdi, IEEE Microw. Wirel. Compon. Lett. **18**, 218-220 (2008).
19. A. Maestrini, J. S. Ward, J. J. Gill, C. Lee, B. Thomas, R. H. Lin, G. Chattopadhyay, and I. Mehdi, IEEE Trans. Microw. Theory Thechn. **58**, 1925-1932 (2010).
20. L. Y. Xu, C. A. Curwen, D. G. Chen, J. L. Reno, T. Itoh, and B. S. Williams, IEEE J. Sel. Top. Quantum Electron. **23**, 1200512 (2017).
21. L. Y. Xu, D. G. Chen, T. Itoh, J. L. Reno, and B. S. Williams, Opt. Express **24**, 24117-24128 (2016).
22. B. S. Williams, S. Kumar, Q. Hu, and J. L. Reno, Opt. Express **13**, 3331-3339 (2005).
23. C. A. Curwen, J. L. Reno, and B. S. Williams, Nat. Photon. **13**, 855-859 (2019).
24. M. I. Amanti, G. Scalari, R. Terazzi, M. Fischer, M. Beck, J. Faist, A. Rudra, P. Gallo, and E. Kapon, New J. Phys. **11**, 125022 (2009).
25. C. A. Curwen, S. J. Addamane, J. L. Reno, M. Shahili, J. H. Kawamura, R. M. Briggs, B. S. Karasik, and B. S. Williams, AIP Adv. **11**, 125018 (2021).
26. H. W. Hubers, H. Richter, R. Eichholz, M. Wienold, K. Biermann, L. Schrottke, and H. T. Grahn, IEEE J. Sel. Top. Quantum Electron. **23** (2017).
27. R. Lang, and K. Kobayashi, IEEE J. Quantum Electron. **16**, 347-355 (1980).
28. R. Adler, Proc. Inst. Radio Eng. **34**, 351-357 (1946).
29. R. Lang, IEEE J. Quantum Electron. **18**, 976-983 (1982).
30. R. P. Green, J. H. Xu, L. Mahler, A. Tredicucci, F. Beltram, G. Giuliani, H. E. Beere, and D. A. Ritchie, Appl. Phys. Lett. **92** (2008).